*Chaotic Modeling and Simulation (CMSIM) 2: 335-348, 2013*

# Nanoindentation for Measuring Individual Phase Mechanical Properties of Sn-Ag-Cu Lead-Free Solders Incorporating Pileup Effects

**Muhammad Sadiq, [1,2,3,5], Jean-Sebastien Lecomte, [4], Mohammed Cherkaoui, [1,2,3]**

[1] George W. Woodruff School of Mechanical Engineering, Georgia Institute of Technology, 801 Ferst Drive NW, Atlanta, GA 30332, USA
[2] University of Lorraine, LEM3 UMR CNRS 7239, île du Saulcy, Metz 57045 France
[3] UMI 2958-Georgia Tech-CNRS Georgia Tech Lorraine, Metz 57070, France
[4] ENSAM-Arts et Métiers ParisTech, LEM3 UMR CNRS 7239, 4 rue Augustin Fresnel, Metz 57078 France
[5] msadiq3@gatech.edu

**Abstract:** Sn-Ag-Cu (SAC) alloys are considered as the best replacements of Sn-Pb alloys which are banned due to the toxic nature of Pb. But, SAC alloys have a coarse microstructure that consists of β-Sn rich and eutectic phases. Nanoindentation is a useful technique to evaluate the mechanical properties at very small length scale. In this work, CSM nanoindentation setup is used to determine the individual phase mechanical properties like Young's modulus and hardness at high temperatures. It is demonstrated that these properties are a function of temperature for both β-Sn rich and eutectic phases. Loadings starting from 500 μN upto 5000 μN are used with 500 μN steps and average values are presented for Young's modulus and hardness. The loading rates applied are twice that of the loadings. High temperatures results in a higher creep deformation and therefore, to avoid it, different dwell times are used at peak loads. The special pileup effect, which is more significant at elevated temperatures, is determined and incorporated into the results. A better agreement is found with the previous studies.

**Keywords:** SAC alloys, Nanoindentation, Young's modulus, Hardness, Pileup effects

## 1. Introduction

Good set of entire mechanical, electrical, chemical and thermal properties are the key elements before classifying any solder to be good for current solder joints. All of these properties were well set for Sn-Pb solder until no restrictions were taken by RoHS and Environmental Protection Agency (EPA), which identified Pb as toxic to both environment and health. This is because Pb and Pb-containing compounds, as cited by EPA, is one of the top 17 chemicals posing the greatest threat to human beings and the environment [1]. Moreover,

Received: 14 April 2012 / Accepted: 28 September 2012

ISSN 2241-0503

current consumer demands and strict governmental legislations [2-4] are pushing the electronics industry towards lead-free solders.

Many lead-free solder alloys are studied by different researchers with wide range of applications. In Abtew's report [2], almost 70 lead-free solders are proposed to replace their lead based counterparts. Most of the newly defined lead-free solders are binary and tertiary alloys [5], out of which, SAC tertiary alloys are considered as the best substitutes [6]. As like many other alloy systems, SAC has also certain limitation due to their coarse microstructure. Iron (Fe), cobalt (Co) and nickel (Ni) are used as potential additives to overcome these limitations [7]. In some studies, indium (In), bismuth (Bi), copper (Cu) and silver (Ag) are used as alloying elements [5]. Before classifying SAC as good substitute, extensive knowledge and understanding of the mechanical behaviour of this emerging generation of lead-free solders is required to satisfy the demands of structural reliability.

Electronic devices once subjected to severe conditions during service exposes solder joints to elevated temperatures. This causes significant evolution of the microstructure of SAC alloys. SAC alloys consists of β-Sn, eutectic Sn phases and Ag-Sn and Cu-Sn InterMetallic Compounds (IMCs). These IMCs are generally hard and brittle in nature which dictates the entire mechanical properties of the solder joints. Exposures to high temperatures causes thermal coarsening due to which the size of these IMCs grow and further deteriorate the solder joints and hence alters the structural reliability of the whole assembly. Rare-earth elements, known as the vitamins of metals, are used in different studies to control this thermal coarsening with significant results [8-11]. All these elements refine the grain size leading to a fine microstructure which ultimately improves the mechanical properties of SAC lead-free solders including yield stress and tensile strength [10-11].

The fast introduction of lead-free solders without deep knowledge of their behaviour has caused many problems in the current electronics industry. Therefore, good understanding of SAC alloys is required to explore the mechanical properties and enhance the solder joint reliability. The main focus of this work is to measure the individual phase properties like Young's modulus and hardness of SAC alloys for eutectic Sn and β-Sn phases. Many researchers have already attempted to determine the mechanical properties of Sn-Ag and SAC alloys [12-13]. The indenter causes piling up inside the soft Sn-matrix which has been neglected in many studies which makes the results unreliable. In this study, the piling up effect is considered for both phases and evaluated using semi-ellipse method and incorporated into results. Both results, before modification and after modification are provided for comparison.

## 2. Experimental

Solder alloy used in this study is Sn3.0Ag0.5Cu with 96.5 wt % of Sn, 3 wt % of Ag and 0.5 wt % of Cu. Since sample preparation for any kind of experimental study is crucial. Therefore a casting die is used to make the samples using "cast by melt" process with many advantages. This die gives almost final shape to the samples with minimum of final machining required.

Almost voids-free surface is achieved which is very important for the nanoindentation testing. During casting the microstructure of the testing samples is controlled using specified cooling rate which is about 3°C/s. A temperature of 260°C was kept in the oven and the die was heated for about 45 minutes before putting the molten metal into it. The 200g ingots were put in a crucible and then placed in the oven at 260°C for about 25 minutes. Water at a temperature of 15°C was used for quenching; the cooling rate of the specimens was measured with a K-type thermocouple. Only a small part of the die was dipped in the water to get a slow cooling rate of about 3°C/s, which is close to the actual soldering process. The dog-bone shape specimen is shown in Figure 1 with a thickness of 2mm.

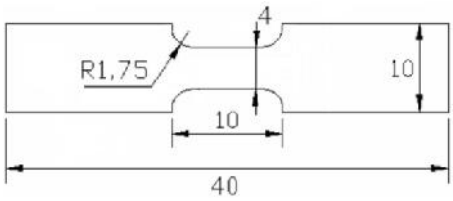


Fig. 1. Dog-bone specimen (all dimensions in mm)

Specimens were mechanical polished with silicon discs and 1 micron diamond paste. Chemical etching was performed for a few seconds using a 5% hydrochloric acid and 95% ethanol solution in order to distinguish between different phases. Figure 2 shows an SEM micrograph and Optical microscope (OM) micrograph taken before the nanoindentation. An Oxford EDS system placed in the SEM enabled to realize elemental mappings for every specimen.

Nanoindentation tests were carried out by using a nanoindenter XP equipped with a Berkovich-84 diamond indenter. The resolutions of the loading and displacement systems are 50 nN and 0.01 nm, respectively. Both of the standard deviation errors of the measured hardness and reduced modulus values for the standard are well less than 1%. The hardness value and reduced modulus values were also extracted from the unloading part of load–depth curves by using Oliver and Pharr method [14].

An acquisition frequency was 10 Hz and poison ratio, assumed, was 0.33. The load applied were 100 µN to 5000 µN with steps of 500 µN. The loading and unloading rates (mN/min) were two times that of load applied (mN). An approach speed of 3000 µN/min was used. As the lead free solders exhibit severe creep deformation, even at room temperature [15], the dwell time at the peak load is defined as 60 seconds in order to completely relieve the creep deformation and also avoid the famous “bulge” or “nose” effect during unloading [16].

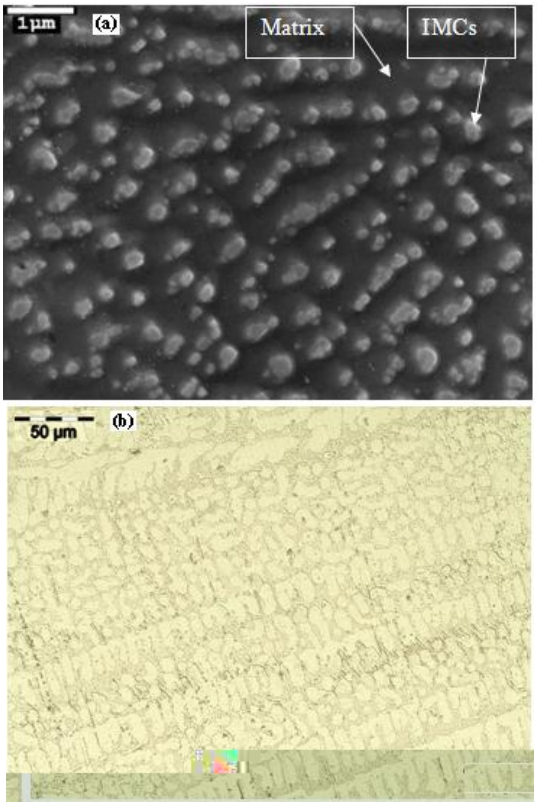


Fig. 2. (a) SEM and (b) Optical Microscope micrographs before nanoindentation

The selection of position to indent was controlled under a high-resolution Optical Microscope (OM), by which various phases can be distinguished. OM was also applied after the indentation to confirm the indenter location and avoid the grain boundary effects. For each specimen, 9 points (3X3 arrays) were tested. Both phases, eutectic and β-Sn, were selectively indented by the visual matrix method. Same tested zones were studied after the indentation testing with Atomic Force Microscope (AFM).

Afterwards, Scanning Electron Microscope (SEM) and Energy Dispersive Spectroscopy (EDS) were used to confirm the chemical composition of each phase. Further, because the Young's modules and hardness for each phase is different, curves for eutectic phase and β-Sn phase can be distinguished from the test array.

## 3. Results and discussion

This is well known in the nanoindentation testing that the typical load-depth curve has significant importance for extracting the overall results. Most importantly, the slope of the unloading portion of the curve is used in almost all

calculations. As discussed earlier, SAC alloys are famous for their low creep resistance and hence quite vulnerable to creep, due to which the pile-up effects happens which causes the "bulge effect" in both β-Sn and eutectic-Sn phases. It is important to avoid this "bulge effect" as it may alter the credibility of final results. Different loads were tested to avoid this effect but it still exists as shown in Figure 3.

Moreover, in order to investigate the creep effects on the mechanical properties, different holding times were used. In comparison to Sn matrix, the IMCs are expected to be resistant to the creep effect. In some cases, there is some bulge effect, but it can be concluded that this is because of the Sn matrix in which these particles are finally embedded.

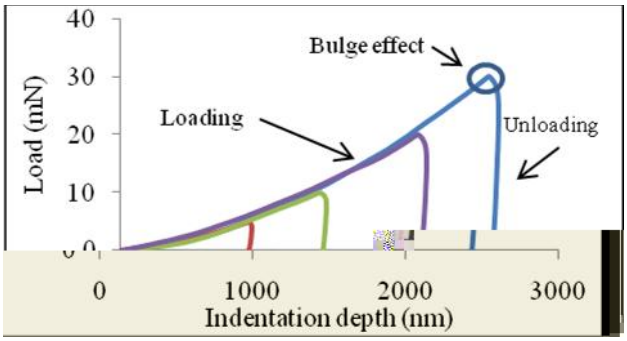


Fig. 3. Load-displacement curves with no holding time

Both β-Sn and eutectic Sn phases were subjected to indentation testing. The load-time history for the entire testing is shown in Figure 4.At a peak load of 5000μN, a 60 seconds dwell time was used to avoid the bulge effect. Solder joints are exposed to high temperatures during service. This causes thermal coarsening of IMCs, due to which, their size grows as the diffusion rate of Ag and Cu into Sn increases at elevated temperatures. It is of utmost importance to understand and explore the individual phase mechanical properties up to a homologues temperature of at least $0.4T_m$, where $T_m$ is the melting point of SAC alloy.

The Load-Depth curves for individual phases at 20°C, 45°C and 85°C are given in Figures 5-7 respectively. In this case, the bulge effect is negligible. Quite useful information can be extracted from these curves. It is important to visualize that the elastic deformation in both phases is quite small which makes the unloading curve almost straight (vertical). Moreover, as also described by the other researchers, indentation depth in eutectic phase is significantly smaller than the β-Sn phase [15]. This effect was also confirmed when the hardness of both phases were compared, eutectic phase being harder than β-Sn phase. This could be the effect of diffusion of Ag and Cu in Sn in the eutectic zone. For confirmation of the testing zone, the tested specimens were taken under the AFM. High resolution images were collected as provided in Figure 8 for the

testing performed over eutectic zone in SAC alloy. Different size of indentation represents different loadings applied during testing.

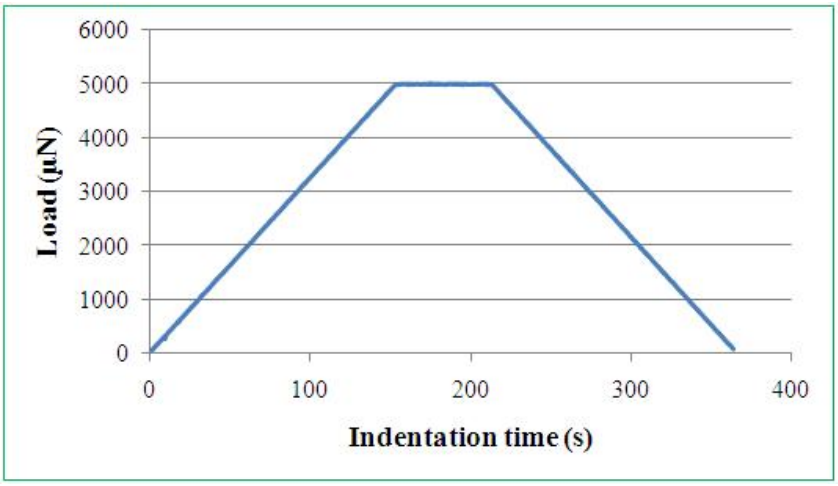


Fig. 4. Load-time history during indentation testing with 60 seconds dwell time

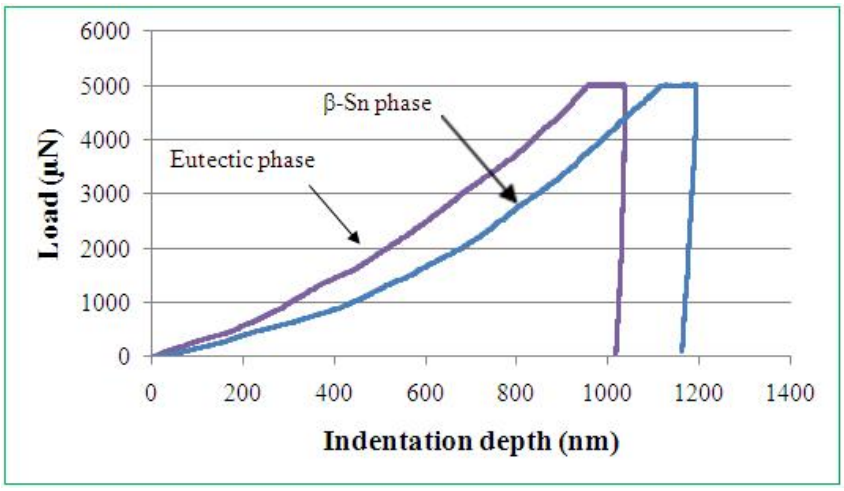


Fig. 5. Load-displacement curves for Eutectic and β-Sn phases at 20°C

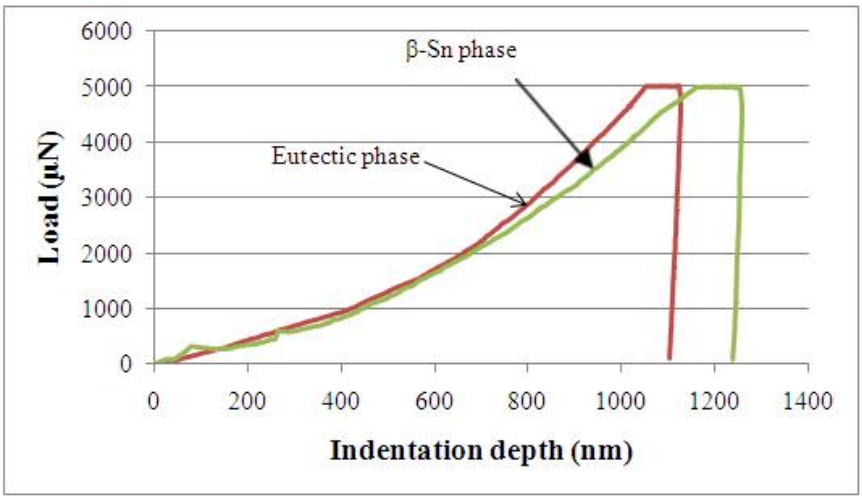


Fig. 6. Load-displacement curves for Eutectic and β-Sn phases at 45°C

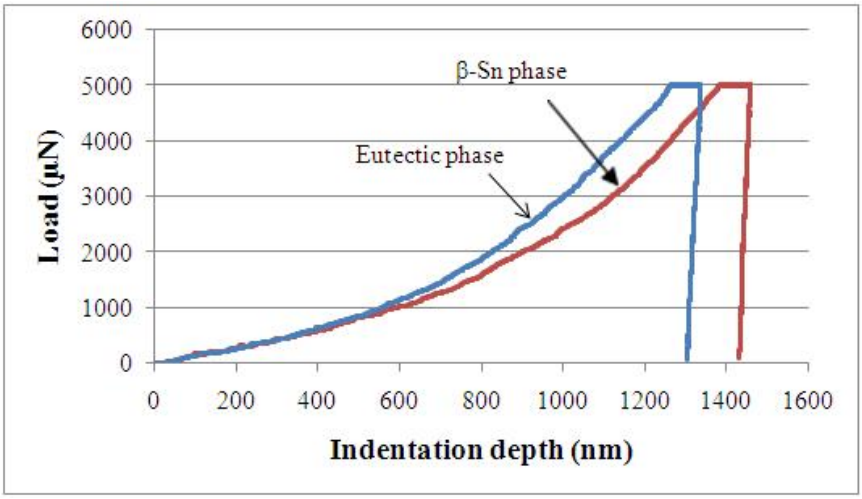


Fig. 7. Load-displacement curves for Eutectic and β-Sn phases at 85°C

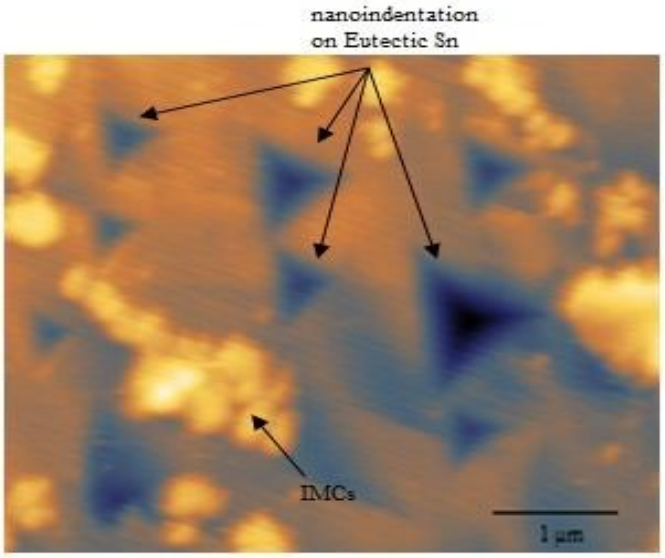


Fig. 8. AFM image after nanoindentation over eutectic zone

## 3. Oliver and Pharr Model

Oliver and Pharr Model (OPM) is extensively used for the solder alloys [14]. Both Young's modulus and hardness are easily extracted using OPM after calculating the reduced modulus $E_r$ as described in equation (1),

$$\frac{1}{E_r} = \frac{\sqrt{®}}{2} \cdot \frac{S}{\sqrt{A_{op}}} \text{.....(1)}$$

where S is the contact stiffness calculated from the slope of the unloading portion of the curve, β is a constant related to the geometry of the indenter, and $A_{op}$ is the oliver-pharr area projected during indentation. At the same time, the reduced Young's modulus could be formulated as,

$$\frac{1}{E_r} = \frac{1-v^2}{E} + \frac{1-v_i^2}{E_i} \text{.....(2)}$$

where E and υ are the Young's modulus and Poisson's ratio of the tested material and $E_i$, $\upsilon_i$ are the Young's modulus and Poisson's ratio for the diamond tip. The values of $E_i$ and $\upsilon_i$ used in this study were 1141 GPa and 0.07, respectively as used in most of the studies [8] and the Poisson's ratio of each phase, i.e., β-Sn and eutectic Sn phase was approximated to be 0.33 which was consistent with the previous studies [8]. Hardness (H) of the material, on the other hand, can be determined by (3) where $F_{max}$ is the peak indentation load and $A_{op}$ is the projected contact area

$$H = \frac{F_{\max}}{Aop} \text{.....(3)}$$

$$A_{op} = 24.5h_c^{\,2} + \sum_{i=1}^{8} C_i h_c^{\frac{1}{2i}} .....(4)$$

Table I. Constant "C" values for berkovich-BK indenter tip

| $C_0$ | $C_1$ | $C_2$ | $C_3$ | $C_4$ | $C_5$ |
|---|---|---|---|---|---|
| 24.5 | 10.31 | -16.03 | 24.45 | -7.32 | 5.12 |

where C is the constant depending on the indenter type and shape and are given in Table I for Berkovich-BK indenter tip. $h_c$ is the contact depth which is smaller than the theoretical depth due to the sinking effect of the specimen under indenter.

Both Young's modulus and hardness are determined and provided for eutectic and β-Sn phases in Table II. These are the results before pile-up effects. Almost no change was investigated with varying loading and loading rates. This is consistent with other studies [15].

Table II. Individual phases Young's modulus and hardness before pileup effects

| **Phase** | **Young's modulus (Gpa)** | **Hardness (Gpa)** |
|---|---|---|
| Eutectic-Sn | 60±3 | 0.35±0.04 |
| β-Sn | 54±4 | 0.30±0.045 |

## 4. Pileup area calculations

Assuming that the projected contact area, $A_c$, determined at contact depth, hc, traces an equilateral triangle of side b, then for a perfect Berkovich tip,

$$A_c = 24.56h_c^{\,2} .....(5)$$

There are semi-elliptical portions at each side of the triangle as shown in Figure 9. The area of each semi-elliptical pile-up projected contact area is $\frac{\pi b}{4} a_i$ and the total pile-up contact area is, therefore,

$$A_{pu} = \frac{®b}{4} \sum a_i .....(6)$$

where the summation is over three semi-elliptical projected pile-up lobes and $a_i$ being the measurement of piling up width on three surface (sides) of the equilateral triangles [2]. The AFM images are analyzed in image-plus to trace the surface profiles and are given in Figure 10. Knowing then the contact area from the Oliver–Pharr method, the total or true contact area for an indent can be obtained as:

$$A = 24.5h_c^{\,2} + \sum_{i=1}^{8} C_i h_c^{\frac{1}{2i}} + \frac{®b}{4} \sum a_i .....(7)$$

Incorporating this new pileup area into the original OPM as presented in equations (1) and (3) becomes,

$$\frac{1}{E_r} = \frac{\sqrt{®}}{2} \cdot \frac{S}{\sqrt{A_{op} + A_{pu}}} \text{.....(8)}$$

$$H = \frac{F_{\max}}{A_{op} + A_{pu}} \text{.....(9)}$$

The hardness and indentation modulus measured for eutectic and β-Sn phases are shown in Table III after incorporating the pileup effects. These results are in a better agreement with the previous studies [12]. This collection of data allows for comparison of mechanical properties of different phases, where all of the samples were prepared and tested in the same manner.

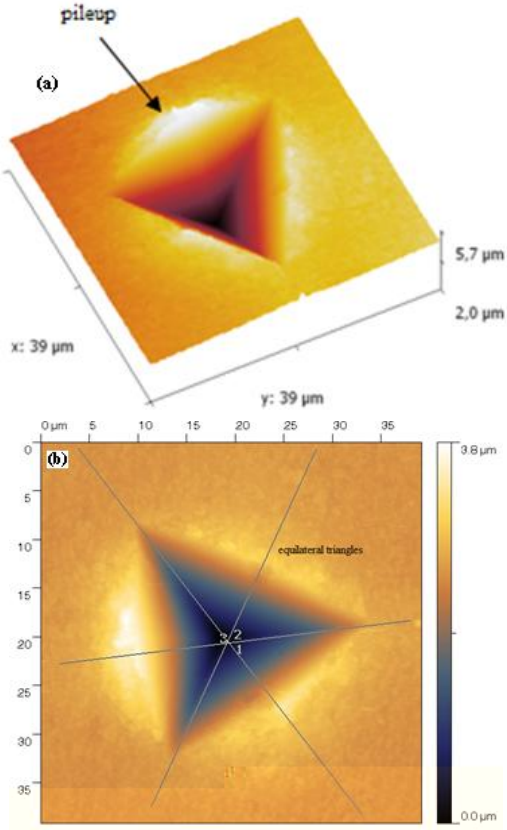


Fig. 9. (a) Pileup schematic and (b) equilateral triangles after testing

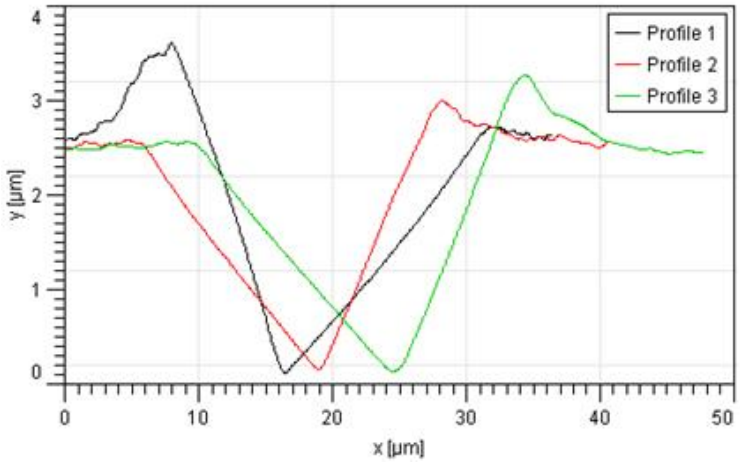


Fig. 10. Pileup profiles for equilateral triangles

Table III. Young's modulus and hardness after pileup effects

| **Phase** | **Young's modulus (Gpa)** | **Hardness (Gpa)** |
|---|---|---|
| Eutectic phase | 49±2 | 0.25±0.05 |
| β-Sn phase | 45±3 | 0.20±0.06 |

Both Young's modulus and hardness were also determined along the indentation depth with experiencing only small variations which is also consistent with [12]. The average values for the Young's modulus for eutectic phase, along the indentation depth, are determined to be 51 GPa whereas for β-Sn it is 48 GPa. Similarly, the average values for hardness, along the depth, for eutectic phase are determined to be 0.26 GPa whereas for β-Sn it is 0.22 GPa. The average values are taken from 100 nm to 500 nm depth. These values are taken after considering the pileup effects.

Similarly, summarized results for β-Sn and eutectic phases for Young's modulus and hardness at elevated temperatures are given in Tables IV-V respectively.

Table IV. Mechanical properties for β-Sn phase at different temperatures

| **Temperature (° C)** | **Young's modulus (GPa)** | **Hardness (GPa)** |
|---|---|---|
| 45 | 37.42 ±2.1 | 0.10 ±0.03 |
| 65 | 36.21 ±3.2 | 0.095 ± 0.025 |
| 85 | 34.85 ±3.5 | 0.087 ± 0.027 |

Table V. Mechanical properties for Eutectic phase at different temperatures

| Temperature (°C) | Young's modulus (GPa) | Hardness (GPa) |
|---|---|---|
| 45 | 42.83 ±2.7 | 0.19 ±0.040 |
| 65 | 43.72 ±2.2 | 0.17 ± 0.025 |
| 85 | 51.85 ±4.5 | 0.11 ± 0.027 |

Like the other phases of SAC alloys, the nanoindentation setup is also used for IMCs. These IMCs are hard and brittle as compare to the other phases in the same specimens. The EDS elemental mapping is used to verify the compositions of these IMCs before implementing the nanoindentation.

The AFM micrograph is given in Figure 11 in which the indentation is carried out on IMCs. These images are collected just after the indentation process. The results for Young's modulus and hardness for both $Ag_3Sn$ and $Cu_6Sn_5$ IMCs are provided in Table VI, with good comparison to the previous studies [17]. This is important to mention that the pileup effect is very small for these particles which is consistent with previous studies and therefore is neglected for IMCs.

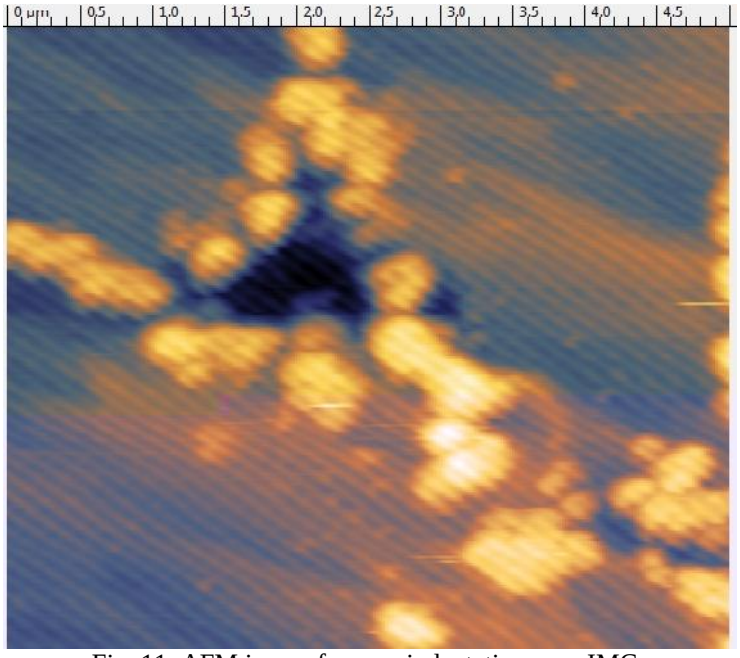


Fig. 11. AFM image for nanoindentation over IMCs

Table VI. Mechanical properties for IMCs

| IMCs | Young's Modulus (GPa) | Hardness (GPa) |
|---|---|---|
| $Ag_3Sn$ | $74 \pm 3$ | $3.32 \pm 0.2$ |
| $Cu_6Sn_5$ | $91 \pm 5$ | $5.8 \pm 0.6$ |

## 5. Conclusions

A detailed study was carried out to explore the individual phase mechanical properties using nanoindentation for the SAC alloy which is considered as potential substitute for SnPb solder. Varying loads and loading rates were used to avoid the typical "bulge effects" and hence make the results more reliable. Piling effect, already ignored by many researchers, is calculated and incorporated into the Oliver-Pharr model. Image-Plus software is used to treat the indentation images taken with AFM after testing and hence plot the individual surface profiles to better explain the material behaviour. It is concluded that this pileup area play a major role in calculating the real results particularly for the soft Sn phase which has more pileup than the eutectic phase. Young's modulus and hardness were also determined along the indentation depth and almost no change was observed which is consistent with previous studies. Different temperatures are used and the load-depth curves are plotted for individual phases. It is noticed that both Young's modulus and hardness reduces with increasing temperatures for both phases.

## References

1. E.P. Wood, K.L. Nimmo, "In search of new lead-free electronic solders" *J. Elect. Mat.* Vol. 23 No. 8 (1994) 709–713

2. Y. Sun et al. "Nanoindentation for measuring individual phase mechanical properties of lead free solder alloy" *J. Mat. Sci: Mater Electron* 19: (2008) 514–521

3. K.N. Tu, A.M. Gusak, M. Li, "Physics and materials challenges for lead-free solders" *J. Appl. Phys.* Vol. 93 No. 3, (2003) 1335-1353

4. M. Abtew, G. Selvaduray, "Lead-free solders in microelectronics" *Mater. Sci. Eng.* Vo. 27 No. 5 (2000) 95-141

5. D. Q. Yu, J. Zhao, L. Wang, "Improvement on the microstructure stability, mechanical and wetting properties of Sn-Ag-Cu lead-free solder with the addition of rare earth elements" *J. alloys and compounds* Vol. 376 No. 1-2 (2004) 170-175

6. M. A. Rist, W. J. Plumbridge, S. Cooper, "Creep-constitutive behavior of Sn-3.8Ag-0.7Cu solder using an internal stress approach" *J. Elect. Mat.* Vol. 35, No. 5 (2006) 1050-1058

7. I. E. Anderson et al. "Alloying effects in near-eutectic Sn-Ag-Cu solder alloys for improved microstructural stability" *J. Elect. Mat.* Vol. 30 No. 9, 2001, 1050-1059

8. Anon, "Rare-Earth solders Make Better Bounds", *Photonics Spectra*, Vol. 36, No. 5 (2002), 139

9. M. Pei and J. Qu, "Effect of Lanthanum Doping on the Microstructure of Tin-Silver Solder Alloys" *J. Elect. Mat.* Vol. 37 No. 3 (2008) 331-338

10. X. Ma, Y. Qian, F. Yoshida, "Effect of La on the Cu-Sn intermetallic compound (IMC) growth and solder joint reliability" *J. alloys and compounds*, Vol. 334 No. 1-2 (2002), 224-227
11. C. M. L. Wu, Y. W. Wong, "Rare-earth additions to lead-free electronic solders" *J. Mater Sci. Mater Electron* Vol. 18 No. 1-3 (2007) 77–91
12. X. Deng, et al., "Deformation behavior of (Cu, Ag)-Sn intermetallics by nanoindentation" *Acta Mater.* Vol. 52 No. 14, (2004) 4291-4303
13. H. Rhee, J.P. Lucas, K.N. Subramanian, "Micromechanical characterization of thermomechanically fatigued lead-free solder joints" *J. Mater. Sci. Mater. Electron.* Vol. 13 No. 8 (2002), 477-484
14. W.C. Oliver, G.M. Pharr, "An improved technique for determining hardness and elastic modulus using load and displacement sensing indentation experiments" *J. Mater. Res.* Vol. 7 No. 6 (1992) 1564–1583
15. Gao F., Takemoto T., "Mechanical properties evolution of Sn-3.5Ag based lead-free solders by nanoindentation" , *Materials Letters* Vol. 60 No. 19 (2006) 2315–2318
16. *Y.T. Cheng, C.M. Cheng,* "Scaling, dimensional analysis, and indentation measurements" *Mater. Sci. Eng. R Rep.* 44 (2004) 91-149
17. R. R. Chromik, R. P. Vinci, S. L. Allen and M. R. Notis "Nanoindentation measurements on Cu–Sn and Ag–Sn intermetallics formed in Pb-free solder joints" *Journal of Materials Research* 18 (2003), 2251-2261